

1 **Rapid growth in nitrogen dioxide pollution over Western China, 2005-2013**

2 Y.-Z. Cui<sup>1</sup>, J.-T. Lin<sup>2</sup>, C. Song<sup>3</sup>, M.-Y. Liu<sup>2</sup>, Y.-Y. Yan<sup>2</sup>, Y. Xu<sup>1</sup> and B. Huang<sup>1,4</sup>

3 <sup>1</sup>Department of Geography and Resource Management, The Chinese University of  
4 Hong Kong, Shatin, NT, Hong Kong

5 <sup>2</sup>Laboratory for Climate and Ocean-Atmosphere Studies, Department of Atmospheric  
6 and Oceanic Sciences, School of Physics, Peking University, Beijing 100871, China

7 <sup>3</sup>Department of Geography, University of California, Los Angeles, Portola Plaza, Los  
8 Angeles, CA 90095, United States

9 <sup>4</sup>Institute of Space and Earth Information Science, The Chinese University of Hong  
10 Kong, Shatin, NT, Hong Kong

11 Correspondence: J.-T. Lin (linjt@pku.edu.cn) and B. Huang (bohuang@cuhk.edu.hk)

12 Short title: Rapidly growing NO<sub>2</sub> over Western China

13

14 **Abstract**

15 Western China has experienced rapid industrialization and urbanization since the  
16 implementation of the National Western Development Strategies (the “Go West”  
17 movement) in 1999. This transition has affected the spatial and temporal characteristics  
18 of nitrogen dioxide (NO<sub>2</sub>) pollution. In this study, we analyze the trends and variability  
19 of tropospheric NO<sub>2</sub> vertical column densities (VCDs) from 2005 to 2013 over Western  
20 China, based on a wavelet analysis on monthly mean NO<sub>2</sub> data derived from the Ozone  
21 Monitoring Instrument (OMI) measurements. We focus on the anthropogenic NO<sub>2</sub> by  
22 subtracting region-specific “background” values dominated by natural sources. After  
23 removing the background influences, we find significant anthropogenic NO<sub>2</sub> growth  
24 over Western China between 2005 and 2013 ( $8.6 \pm 0.9\% \text{ yr}^{-1}$  on average, relative to  
25 2005), with the largest increments ( $15\% \text{ yr}^{-1}$  or more) over parts of several city clusters.  
26 The NO<sub>2</sub> pollution in most provincial-level regions rose rapidly from 2005 to 2011 but  
27 stabilized or declined afterwards. The NO<sub>2</sub> trends were driven mainly by changes in

1 anthropogenic emissions, as confirmed by a nested GEOS-Chem model simulation and  
2 a comparison with Chinese official emission statistics. The rate of NO<sub>2</sub> growth during  
3 2005-2013 reaches  $11.3 \pm 1.0\% \text{ yr}^{-1}$  over Northwestern China, exceeding the rates over  
4 Southwestern China ( $5.9 \pm 0.6\% \text{ yr}^{-1}$ ) and the three well-known polluted regions in the  
5 east ( $5.3 \pm 0.8\% \text{ yr}^{-1}$  over Beijing-Tianjin-Hebei,  $4.0 \pm 0.6\% \text{ yr}^{-1}$  over the Yangtze River  
6 Delta, and  $-3.3 \pm 0.3\% \text{ yr}^{-1}$  over the Pearl River Delta). Subsequent socioeconomic  
7 analyses suggest that the rapid NO<sub>2</sub> growth over Northwestern China is likely related  
8 to the fast developing resource- and pollution-intensive industries along with the “Go  
9 West” movement as well as relatively weak emission controls. Further efforts should  
10 be made to alleviate NO<sub>x</sub> pollution to achieve sustainable development in Western  
11 China.

12

## 1 **1 Introduction**

2 Nitrogen oxides ( $\text{NO}_x = \text{NO} + \text{NO}_2$ ) are major constituents in tropospheric chemistry,  
3 leading to ozone formation, acid deposition, and particulate matter pollution.  $\text{NO}_x$  are  
4 emitted into the troposphere from anthropogenic activities (thermal power plants,  
5 transportation, industries, and residential use) and natural sources (lightning, open fires,  
6 and soil) (Lin, 2012; Russell et al., 2012). Rapid economic development and  
7 urbanization across China in recent decades have caused serious air pollution problems,  
8 with  $\text{NO}_x$  becoming the fastest growing air pollutant in China over the last two decades  
9 (Richter et al., 2005; Zhang et al., 2012; Zhao et al., 2013).

10 Vertical column densities (VCDs) of tropospheric  $\text{NO}_2$  retrieved from various satellite  
11 instruments have been used widely to study  $\text{NO}_x$  pollution over China (Richter et al.,  
12 2005; van der A et al., 2006; He et al., 2007; Wang et al., 2007b; Zhang et al.,  
13 2007b; Zhang et al., 2012; Gu et al., 2013; Huang et al., 2013; Lin et al., 2014b). Satellite  
14 observations provide a tool to infer patterns of anthropogenic and natural  $\text{NO}_x$   
15 emissions (Zhang et al., 2007a; Stavrou et al., 2008; van der A et al., 2008; Zhang et  
16 al., 2009b; Zhao and Wang, 2009; Li et al., 2010; Lin et al., 2010b; Lamsal et al., 2011; Lin,  
17 2012; Wang et al., 2012; Reuter et al., 2014; Lin et al., 2015). They are also useful to  
18 analyze the large variations in  $\text{NO}_x$  pollution during several short-term socioeconomic  
19 events, such as the Sino-African summit, Beijing Olympic Games, Shanghai Expo,  
20 Guangzhou Asian Games, Chinese economic recession and Chinese New Year (Wang  
21 et al., 2007a; Mijling et al., 2009; Wang et al., 2009; Witte et al., 2009; Hao et al.,  
22 2011; Lin and McElroy, 2011; Lin et al., 2013).

23 Most of prior studies have focused on Eastern China, with little attention paid to  
24 Western China. As shown in Fig. 1, Western China is specified here as the vast region  
25 covering six provinces (Gansu, Guizhou, Qinghai, Shaanxi, Sichuan and Yunnan), five  
26 provincial-level autonomous regions (Guangxi, Inner Mongolia, Ningxia, Tibet and  
27 Xinjiang), and one provincial-level municipality (Chongqing City). Western China has  
28 experienced significant socioeconomic changes following the National Western  
29 Development Strategies (the “Go West” movement) launched by the Chinese

1 government in 1999. Over the last decade, the rates of industrialization and urbanization  
2 in Western China has accelerated (Deng and Bai, 2014). Western China is rich in natural  
3 resources, such as water, coal, natural gas, petroleum, and minerals. With the  
4 adjustment of regional development strategy at a national level, those energy-intensive  
5 industries formerly located in Eastern China have been encouraged to move westward  
6 (Zhao et al., 2015), although the ecosystems of Western China may be more fragile than  
7 those of Eastern China (Shao and Qi, 2008;Chen et al., 2010;Bai et al., 2014;Zhao et  
8 al., 2015). Although the “Go West” movement is beneficial for local industrial and  
9 economic development in Western China, it may have led to unintended environmental  
10 impacts that have yet to be understood. The short lifetime of tropospheric NO<sub>2</sub> (hours  
11 to a day), its strong link and rapid response to emissions, and the availability of high-  
12 quality satellite measurements allow evaluating pollution changes and the possibility of  
13 sustainable development in Western China. Satellite measurements are particularly  
14 important in lack of sufficient ground-based measurements.

15 This study investigates the spatiotemporal variations of tropospheric NO<sub>2</sub> VCDs  
16 between October 2004 and May 2014 over Western China and potential human  
17 influences, by analyzing the monthly Royal Netherlands Meteorological Institute  
18 (KNMI) Ozone Monitoring Instrument (OMI) NO<sub>2</sub> data (DOMINO v2). We apply a  
19 wavelet decomposition analysis to reveal the long-term trends of tropospheric NO<sub>2</sub> over  
20 Western China. We also use a nested GEOS-Chem simulation and Chinese official  
21 emission statistics to confirm that anthropogenic emissions are the main driver of NO<sub>2</sub>  
22 variations. At last, we discuss the regional differences in NO<sub>2</sub> growths between  
23 Northwestern and Southwestern China and between Western and Eastern China, and  
24 we associate these differences with the driving socioeconomic factors of individual  
25 regions.

## 26 **2 Data and study area**

### 27 **2.1 Satellite data**

28 OMI is onboard the EOS-Aura satellite. The satellite measurements have a pixel size

1 of  $13 \times 24 \text{ km}^2$  at nadir with a local overpass time around 13:40. VCDs of tropospheric  
2  $\text{NO}_2$  are derived in three major steps, including derivation of slant column densities  
3 (SCDs), separation of stratospheric and tropospheric SCDs, and calculation of  
4 tropospheric air mass factors (AMFs) for deduction of the tropospheric VCDs. On a  
5 regional and monthly mean basis, the error of retrieved VCDs is about 30% (a relative  
6 error) plus  $0.7 \times 10^{15} \text{ molecules cm}^{-2}$  (an absolute error) (Boersma et al., 2011; Lin and  
7 McElroy, 2011). More detailed algorithms and error descriptions involved in retrieving  
8 tropospheric  $\text{NO}_2$  VCDs can be found in Boersma et al. (2007) and Boersma et al.  
9 (2011).

10 We mapped the level-2 DOMINO v2 product  
11 (<http://www.temis.nl/airpollution/no2.html>) to a  $0.25^\circ \times 0.25^\circ$  grid, and then averaged  
12 daily data to produce monthly mean VCD values. We used data from October 2004 to  
13 May 2014 for the present analysis. For data quality control, we excluded pixels with a  
14 cloud radiance fraction  $> 50\%$  or affected by row anomaly (Boersma et al., 2011). We  
15 filled the missing monthly mean values in some grid cells using values in the adjacent  
16 years; the impact on the trend analysis is found to be small by sensitivity analyses on  
17 the respective GEOS-Chem simulation results (see Sect. 4.2.2).

## 18 **2.2 GEOS-Chem Modeling**

19 We used the nested GEOS-Chem chemical transport model version 9-02, on a  $0.667^\circ$   
20  $\text{long.} \times 0.5^\circ \text{ lat.}$  grid with 47 vertical layers, to simulate the tropospheric  $\text{NO}_2$  and other  
21 pollutants over Asia (Chen et al., 2009). The model is run with the full  $\text{O}_x\text{-NO}_x\text{-VOC-}$   
22  $\text{CO-HO}_x$  gaseous chemistry and online aerosol calculations, and it is driven by the  
23 GEOS-5 assimilated meteorology from the NASA Global Modeling and Assimilation  
24 Office. Vertical mixing in the planetary boundary layer follows the non-local  
25 parameterization scheme implemented by Lin et al. (2010b). Convection is simulated  
26 with a modified Relaxed Arakawa-Schubert scheme (Rienecker et al., 2008). Lateral  
27 boundary conditions of the nested model are updated every 3 h by results from  
28 corresponding global modeling on a  $5^\circ \text{ long.} \times 4^\circ \text{ lat.}$  grid.

1 Chinese anthropogenic emissions of NO<sub>x</sub> and other species adopt the monthly MEIC  
2 inventory with a base year of 2008 ([www.meicmodel.org](http://www.meicmodel.org)). The spatial resolution of  
3 MEIC used in the simulation is 0.667° long. × 0.5° lat., according to the model grid.  
4 We further scaled monthly anthropogenic NO<sub>x</sub> emissions to other years, by applying  
5 the ratios of monthly DOMINO v2 NO<sub>2</sub> VCDs in those years over the VCDs in the  
6 respective months of 2008. The scaling with OMI data was done at the model resolution,  
7 after regridding the satellite data from the 0.25° long. × 0.25° lat. resolution. Emissions  
8 for other Asian regions follow the INTEX-B inventory (Zhang et al., 2009a). Other  
9 model setups are described in Lin et al. (2015).

10 Due to limited meteorological inputs, model simulations were conducted from 2004 to  
11 April 2013. The first simulation year was used for model spin-up, and results from 2005  
12 onward were analyzed in the present analysis. In the following order, modeled vertical  
13 profiles of NO<sub>2</sub> were averaged over 13:00 – 15:00 local time, regridded to a 0.25° ×  
14 0.25° grid, sampled in locations and days with valid OMI data, applied with the  
15 DOMINO averaging kernel (AK), and then averaged to derive monthly mean VCD  
16 values. The use of AK was to eliminate the effect of differences in NO<sub>2</sub> vertical profiles  
17 between GEOS-Chem and TM4 (that provides the priori profiles for the DOMINO  
18 retrieval). Following our previous work (Lin et al., 2010a; Lin, 2012), we regridded the  
19 pixel-specific AK to the 0.25° × 0.25° grid. Modeled VCDs data without applying the  
20 AK are also analyzed in Sect. 4.2.2 to test the effects of data sampling and temporal  
21 interpolation.

### 22 **2.3 Official anthropogenic emission and socioeconomic data**

23 We took Chinese official provincial-level NO<sub>x</sub> emission inventories for 2007 and 2010-  
24 2013 to compare with trends in OMI NO<sub>2</sub>. Chinese central government commenced its  
25 official estimate of anthropogenic NO<sub>x</sub> emissions following the first nationwide  
26 pollution census in 2007 (The first nationwide pollution census committee, 2011). NO<sub>x</sub>  
27 emissions in 2010-2013 were also based on the estimating system of the first pollution  
28 census, allowing for a consistent comparison throughout time. We also included the

1 official emission targets aimed for 2015 from the 12<sup>th</sup> Five-Year Plan (2011-2015), a  
2 well-known socioeconomic planning step of China. We obtained all socioeconomic  
3 data from the China Statistical Yearbooks Database  
4 (<http://tongji.cnki.net/overseas/engnavi/navidefault.aspx>).

## 5 **2.4 Study area**

6 Figure 1 highlights the study area in China. We extracted provincial and regional NO<sub>2</sub>  
7 data according to their administrative divisions. We separated Western China into two  
8 sub-regions, including Northwestern China (Gansu, Inner Mongolia, Ningxia, Qinghai,  
9 Shaanxi and Xinjiang) and Southwestern China (Chongqing, Guangxi, Guizhou,  
10 Sichuan and Yunnan). Tibet is excluded from the present analysis due to lack of  
11 socioeconomic data. We also selected three key regions from Eastern China for  
12 comparisons with Western China: the Beijing-Tianjin-Hebei region (BTH, including  
13 Beijing, Tianjin and Hebei Province), the Yangtze River Delta (YRD, including  
14 Shanghai, Jiangsu Province and Zhejiang Province) and the Pearl River Delta (PRD,  
15 part of Guangdong Province).

## 16 **3 Methods**

### 17 **3.1 Determining areas dominated by anthropogenic NO<sub>2</sub>**

18 This study is focused on areas that have been subjected to significant changes in  
19 anthropogenic NO<sub>x</sub> emissions. Since NO<sub>x</sub> are emitted from both anthropogenic and  
20 natural sources (Lin, 2012), we exploited their distinctive seasonal patterns to determine  
21 areas dominated by anthropogenic sources.

22 Over China, anthropogenic emissions tend to maximize in winter, although the seasonal  
23 variation is often within 20% (Zhang et al., 2009a). Soil and lightning emissions exhibit  
24 summer maxima with very low values in winter. Biomass burning emissions of NO<sub>x</sub>  
25 are negligible over China (Lin, 2012). In addition, the lifetime of NO<sub>x</sub> in winter is  
26 several times longer than in summer. Therefore the NO<sub>2</sub> VCDs are the lowest in summer  
27 and the highest in winter over the areas dominated by anthropogenic sources, while the  
28 opposite seasonality occurs over the regions dominated by natural emissions (Lin,

1 2012). Furthermore, lightning and soil emissions are mostly independent of direct  
2 anthropogenic influences for 2005-2013, albeit with certain effects from changes in  
3 climate and/or land use. There is no evidence that these natural emissions underwent  
4 significant trends from 2005 to 2013. By comparison, anthropogenic emissions have  
5 exhibited dramatic changes along with the rapid socioeconomic development, and these  
6 changes have affected the seasonality of NO<sub>2</sub>.

7 Figure 2(a) shows the seasonal variation in OMI NO<sub>2</sub> VCDs, averaged over 2005-2013,  
8 for each 0.25° x 0.25° grid cell in Western China; all grid cells are sorted according to  
9 their 9-year mean NO<sub>2</sub> values. Once a grid cell is ordered, its monthly NO<sub>2</sub> values are  
10 averaged over 2005-2013 to obtain a 9-year mean monthly climatological dataset with  
11 12 values. Finally, the monthly climatological values are converted to their reverse  
12 ranks (from 1 to 12), for improved illustration across all grid cells. Figure 2(a) shows  
13 that for grid cells with 9-year mean NO<sub>2</sub> VCDs below 1.0 x 10<sup>15</sup> molecules cm<sup>-2</sup>, NO<sub>2</sub>  
14 generally experiences summer maxima and winter minima, reflecting the dominance of  
15 natural sources. In contrast, grid cells with 9-year mean NO<sub>2</sub> VCDs above 1.0 x 10<sup>15</sup>  
16 molecules cm<sup>-2</sup> exhibit winter maxima, due to the dominance of anthropogenic  
17 emissions as well as a longer lifetime. van der A et al. (2006) also found that over 1996–  
18 2005, polluted Eastern China experienced NO<sub>2</sub> maxima in winter due to large  
19 anthropogenic emissions while much cleaner western China experienced summer  
20 maxima due to natural sources. Similar results were shown by Lin (2012) who  
21 compared polluted and cleaner regions in Eastern China in 2006.

22 Figure 2(b) further shows the standard deviation (SD) of monthly OMI NO<sub>2</sub> VCDs year  
23 by year for each 0.25° x 0.25° grid cell in Western China; again, all grid cells are sorted  
24 according to their 9-year mean NO<sub>2</sub> values. Once a grid cell is ordered, the SD is  
25 calculated for each year to obtain a dataset with nine values over 2005-2013. Finally,  
26 the SD values are converted to their reverse ranks (from 1 to 9), for better illustration  
27 across all grid cells. Figure 2(b) shows that grid cells with 9-year mean NO<sub>2</sub> VCDs  
28 above 1.0 x 10<sup>15</sup> molecules cm<sup>-2</sup> exhibit a large growth in SD especially since 2009, as  
29 a result of large growth in anthropogenic emissions that amplified the seasonality. By



1 comparison, grid cells with 9-year mean NO<sub>2</sub> VCDs below  $1.0 \times 10^{15}$  molecules cm<sup>-2</sup>  
2 did not experience such significant changes in SD between 2005 and 2013.

3 Based on the above seasonality analysis, we determined the regions dominated by  
4 anthropogenic emissions as those with 2005-2013 mean NO<sub>2</sub> VCDs exceeding  $1.0 \times$   
5  $10^{15}$  molecules cm<sup>-2</sup>.

### 6 **3.2 Removing contributions from natural sources**

7 To obtain the sole anthropogenic NO<sub>2</sub>, we further subtracted all NO<sub>2</sub> VCDs by certain  
8 “background” values representing the natural influences. Removing the “background”  
9 influences is meaningful for Western China where the NO<sub>2</sub> VCDs are currently not at  
10 an extremely high level (see Sect. 4.2.1).

11 We identified six “background” areas that are away from cities and are supposed to be  
12 dominated by natural emissions (see the hatched areas in Fig. 1), and we assumed NO<sub>2</sub>  
13 VCDs there are all natural. Russell et al. (2012) used the same method to identify  
14 “background” NO<sub>2</sub> over the United States. When calculating the trends of NO<sub>2</sub> in the  
15 grid cells of the chosen human-dominant areas, we subtracted NO<sub>2</sub> VCDs at these grid  
16 cells by the NO<sub>2</sub> value averaged over the nearest “background” region. For all grid cells  
17 in a given province, the corresponding background region is the same and is indicated  
18 in Table 1. The background subtraction was done on a monthly basis to account for  
19 natural variability. We processed the model NO<sub>2</sub> data with the same method.

20 Figure 1 shows that the “background” regions in Western China are normally the  
21 uninhabited areas. Over there, the NO<sub>2</sub> VCDs are only about  $0.4 - 0.5 \times 10^{15}$  molecules  
22 cm<sup>-2</sup> in 2005 (with little interannual variability), lower than NO<sub>2</sub> in the polluted areas  
23 by a factor of 2 – 5 (Table 1). For Eastern China (Table 1), the “background” values are  
24 higher ( $0.7 - 1.2 \times 10^{15}$  molecules cm<sup>-2</sup> in 2005); whereas these values are 6–13 times  
25 lower than the NO<sub>2</sub> VCDs over the three polluted eastern regions (BTH, YRD and PRD).

26 Note that the chosen “background” values may not fully represent the actual natural  
27 contributions to the targeted human-dominant areas. For example, soil emissions may  
28 vary in space due to differences in temperature, radiation, land cover and land use type,

1 and other climatic factors. Lightning emissions of NO<sub>x</sub> may have spatial dependence  
2 as well. The “background” regions may not be totally free from anthropogenic  
3 influences, as a certain amount of NO<sub>x</sub> in the polluted areas may be oxidized to produce  
4 peroxyacyl nitrates (PANs), which can be transported to “background” areas and  
5 converted back to NO<sub>x</sub>. For these reasons, our choice of background values is relatively  
6 rough. Nevertheless, unless the actual natural contributions differ substantially from the  
7 chosen values, which we do not expect to occur on a provincial average, the resulting  
8 effect on our trend calculations should be small, because the chosen background values  
9 are smaller than NO<sub>2</sub> over their corresponding polluted areas by a factor of 2–13 (Table  
10 1). Future work is needed to fully separate the anthropogenic from natural NO<sub>2</sub> for  
11 individual locations.

### 12 **3.3 Wavelet decomposition analysis**

13 Due in part to the short lifetime of NO<sub>x</sub>, the tropospheric NO<sub>2</sub> VCDs respond quickly  
14 to emission changes at various temporal scales, from a general growth along with  
15 socioeconomic development to short-term perturbations such as the Chinese New Year  
16 holidays and the economic recession (Lin and McElroy, 2011; Lin et al., 2013). Also,  
17 uncertainties and sampling biases in the satellite data may introduce additional noises  
18 in the NO<sub>2</sub> monthly time series. If not separated, these short-term variability and noises  
19 may affect linear trend calculations.

20 Here we conducted discrete wavelet transform (DWT) (Daubechies, 1992; Partal and  
21 Küçük, 2006) to distinguish temporal variability of NO<sub>2</sub> at multiple scales. The wavelet  
22 transform is a useful tool for diagnosing the multi-scale and non-stationary processes  
23 over finite space and time periods, with the advantage of localization in the time and  
24 frequency domain (Echer, 2004; Percival and Walden, 2006), suitable for our analysis  
25 of NO<sub>2</sub> trends and variability. Different from the approaches adopted by previous NO<sub>2</sub>  
26 studies (e.g., (van der A et al., 2006)), our wavelet analysis does not require prior  
27 assumptions about seasonality and other temporal scales. As shown in Sect. 3.1, the  
28 magnitude of NO<sub>2</sub> seasonality is correlated to the amount of annual mean NO<sub>2</sub> and  
29 anthropogenic sources, and this information is captured by the wavelet analysis here.

1 The multi-scale analysis in DWT is able to decompose a time series  $f(t)$  into  $n$ -scale  
2 components ( $n$  is the decomposition level):

$$3 \quad f(t) = \sum_{i=1}^n D_i + A_n \quad (1)$$

4 where  $D_i$  is a detail signal (high frequency) at level  $i$  and  $A_n$  is the approximation signal  
5 (low frequency) at the set of maximum level  $n$ . The detail and approximation signals  
6 were generated based on the convolution of time series of wavelet functions and scaling  
7 functions. We chose Meyer orthogonal discrete wavelets as the wavelet functions which  
8 have been used to study ozone column, NDVI and land-cover changes (Abry,  
9 1997;Echer, 2004;Freitas and Shimabukuro, 2008;Martínez and Gilabert, 2009).  
10 Specifically, the approximation and detail signals were derived through an iterative  
11 multi-layer decomposition process. In the first layer of decomposition,  $f(t) = A_1 +$   
12  $D_1$ . Then,  $A_1 = A_2 + D_2$  and  $f(t) = A_2 + D_2 + D_1$ . And so on. The iteration stops  
13 at level  $n = 5$  for all provinces. At level 5, the period of the  $A_5$  time series is longer than  
14 the length of the dataset (116 months). This criterion is typically used in investigating  
15 the long-term trend of a time series (Echer, 2004;Chen et al., 2014). As an example, Fig.  
16 3 presents the wavelet transform result for one grid cell (34.5°N, 108.9°E) in Xi'an City,  
17 Shaanxi Province.

18 As a result, the approximation signal  $A_5$  represents the long-term trend of the original  
19  $\text{NO}_2$  time series (with a period longer than the length of the dataset). Although similar  
20 to the 12-month moving average time series, the  $A_5$  time series is much smoother with  
21 no short-term variability (see the example in Fig. 3). The detail components  $D_1$ - $D_5$   
22 indicate higher-frequency variations, which are not analyzed in this study.

## 23 **4 Results and analysis**

### 24 **4.1 Spatial patterns of tropospheric $\text{NO}_2$ VCDs over China, prior to removing** 25 **“background” influences**

26 Figure 4 shows the spatial distributions of annual average OMI  $\text{NO}_2$  VCDs over China  
27 in 2005, 2012 and 2013. Here the “background” values have not been subtracted. The  
28  $\text{NO}_2$  VCDs exceed a high value of  $6 \times 10^{15}$  molecules  $\text{cm}^{-2}$  in many areas of Central-

1 East China and parts of Western China. Chengdu-Chongqing, Urumqi and Shaanxi-  
2 Guanzhong city clusters are well-known pollution “hot spots” of Western China (see  
3 Fig.1 for region definitions). These “hot spots” have intensified since 2005, as well as  
4 other polluted western areas including Gansu-Ningxia and Inner Mongolia industrial  
5 city clusters. The annual and regional average NO<sub>2</sub> VCDs over Western China has  
6 increased by 51% between 2005 and 2013, higher than the increase at 41% in Central-  
7 East China. The large growth of NO<sub>2</sub> over Western China highlights the necessity of  
8 understanding potential human influences in these regions.

9 Figure 4 also compares the OMI derived and GEOS-Chem modeled annual average  
10 NO<sub>2</sub> VCDs in 2005 and 2012. OMI and model NO<sub>2</sub> share similar spatial and temporal  
11 patterns. Linear regression for model NO<sub>2</sub> as a function of OMI NO<sub>2</sub> reveals that for  
12 any given year, model NO<sub>2</sub> are highly correlated with OMI values in space. Table 2  
13 shows that for the whole China in 2008, the magnitudes of model NO<sub>2</sub> are close to OMI  
14 NO<sub>2</sub> (slope = 1.09, R<sup>2</sup> = 0.88). For other years, the slopes are larger (1.11–1.26),  
15 indicating positive model biases, while the R<sup>2</sup> ranges from 0.86 to 0.90. The scatterplot  
16 in Fig. 4 further confirms the model-OMI consistency in 2012. Similar results are found  
17 for Western China, although the R<sup>2</sup> is smaller, at 0.68–0.76 over 2005–2012. The model  
18 biases in years other than 2008 reflect the nonlinear relation between changes in NO<sub>x</sub>  
19 emissions and changes in NO<sub>2</sub> VCDs (Martin et al., 2003; Valin et al., 2011; Lin, 2012)  
20 that we did not account for when linearly scaling model emissions from MEIC 2008 to  
21 other years based on the interannual variation in OMI NO<sub>2</sub>.

## 22 **4.2 Trends of anthropogenic NO<sub>2</sub> over Western China, after removing** 23 **“background” influences**

### 24 **4.2.1 NO<sub>2</sub> trends**

25 Figure 5 shows OMI and modeled NO<sub>2</sub> trends at individual grid cells over Western  
26 China, by applying a linear regression to the approximation signal *A5* from the wavelet  
27 decomposition. All trend values are normalized relative to the 2005 mean NO<sub>2</sub> VCDs.  
28 All the NO<sub>2</sub> data have been subtracted by its respective “background” values prior to

1 the wavelet analysis. Results are only shown for grid cells with 2005-2013 average NO<sub>2</sub>  
2 VCDs exceeding  $1.0 \times 10^{15}$  molecules cm<sup>-2</sup> and with statistically significant trends (*P*-  
3 value < 0.05 according to an *F*-test). Note that the growth rates without subtracting  
4 “background” values are smaller than the rates with “background” values subtracted by  
5 0.5–2.9%/yr (1.5%/yr on average) over the northwestern provinces and 0.1–1.0%/yr  
6 (0.7%/yr on average) over the southwestern provinces. In addition, the *A5*-based trends  
7 here are similar to the linear trends calculated based on the original NO<sub>2</sub> time series  
8 (not shown). However, as the wavelet transform removes small-scale variability and  
9 noises, we believe the *A5*-based trends are more robust in general.

10 Figure 5(a) shows that OMI NO<sub>2</sub> grew at most grid cells from 2005 to 2013, with a  
11 regional average annual growth at  $8.6 \pm 0.9$  % yr<sup>-1</sup>. NO<sub>2</sub> grew the fastest over the city  
12 clusters, reflecting rapid economic development, urbanization, and population growth.  
13 Parts of Chengdu-Chongqing, Shaanxi-Guanzhong and Urumqi city clusters  
14 experienced NO<sub>2</sub> growth of 15 % yr<sup>-1</sup> or more. Most grid cells in yellow color are  
15 suburban or rural areas, but they also underwent rapid NO<sub>2</sub> growth since 2005 (6 -10 %  
16 yr<sup>-1</sup>).

17 Table 1 shows the trends of OMI NO<sub>2</sub> VCDs from 2005 to 2013, as a percentage of  
18 mean values in 2005, on a provincial basis. NO<sub>2</sub> grew the fastest over Xinjiang, Ningxia  
19 and Qinghai with a growth rate at 15.1%, 12.3% and 11.2% per year, respectively. The  
20 growth rates in Northwestern China (7.5 – 15.1 % yr<sup>-1</sup>) were much greater than the rates  
21 in Southwestern China (4.0 – 7.8 % yr<sup>-1</sup>), primarily as a result of the regional differences  
22 in socioeconomic development (see Sect. 5.2).

23 A comparison of Fig. 5(b) and 5(c) shows that GEOS-Chem generally captures the OMI  
24 NO<sub>2</sub> trends from 2005 to 2012, suggesting that anthropogenic emissions are the main  
25 driver of the observed NO<sub>2</sub> trend. OMI data exhibit stronger growth than modeled data  
26 over North Xinjiang, East and South Inner Mongolia, South Sichuan, East Guizhou and  
27 South Guangxi, whereas the OMI trends are weaker than the modeled trends over most  
28 other regions. The differences between modeled and OMI NO<sub>2</sub> reflect the strong but  
29 nonlinear relation between NO<sub>x</sub> emissions and NO<sub>2</sub> VCDs.

1 To further confirm that anthropogenic emissions are the main driver of the observed  
2 NO<sub>2</sub> trends, we conducted an additional model simulation for 2012 where  
3 anthropogenic emissions are fixed at the 2005 levels (while natural emissions and  
4 meteorology correspond to the 2012 levels). We contrasted the model NO<sub>2</sub> change from  
5 2005 to 2012 in this case to the standard case that has included year-specific  
6 anthropogenic emissions. Table 3 shows that inclusion of anthropogenic emission  
7 changes from 2005 to 2012 leads to large changes in model NO<sub>2</sub>, and keeping  
8 anthropogenic emissions unchanged leads to much reduced changes in NO<sub>2</sub>. The NO<sub>2</sub>  
9 growth reduces from 85.8% to 6.9% averaged over the northwestern provinces and  
10 from 46.8% to -6.3% over Southwestern China.

#### 11 **4.2.2 NO<sub>2</sub> time series**

12 Figure 6 further shows the *A5* monthly time series for individual provinces as a result  
13 of wavelet analyses on OMI NO<sub>2</sub>. All values are normalized with respect to 2005. In  
14 particular, the OMI\_1 time series (black line) results from a wavelet analysis on OMI  
15 NO<sub>2</sub> over Oct 2004 – May 2014. OMI\_1 shows that NO<sub>2</sub> grew rapidly between 2007  
16 and 2011 over all provinces. For Xinjiang, Qinghai and Yunnan, OMI NO<sub>2</sub> increased  
17 continuously from 2005 to 2013. Over other provinces, OMI NO<sub>2</sub> peaked around 2011-  
18 2012 and then stagnated or even slightly declined thereafter. These stagnation or  
19 reduction patterns likely reflect recent effective emission control policies (see Sect. 5.1).

20 Figure 6 also compares the *A5* time series for OMI NO<sub>2</sub> (OMI\_2, green line) and model  
21 NO<sub>2</sub> (GC\_AK, red line) derived from wavelet analyses on the same period from Jan  
22 2005 to Apr 2013. Model results were sampled coincidentally with OMI data and were  
23 applied with the AK. OMI\_2 and GC\_AK do not show a stagnation/reduction feature  
24 as obvious as OMI\_1 after 2011, because of a shorter time series for wavelet  
25 decomposition. OMI\_2 and GC\_AK exhibit similar increasing trends and variability in  
26 most western provinces, consistent with the finding in Sect. 4.2.1 that variations in  
27 anthropogenic emissions (accounted for in the model) were the main driver of NO<sub>2</sub>  
28 changes.

1 Our trend analyses may be affected by missing OMI data and the corresponding  
2 temporal interpolation procedure. To evaluate the effects, we compared two additional  
3 datasets based on model results: GC\_NAK1 (blue line in Fig. 6) represents model NO<sub>2</sub>  
4 on all days without applying the AK, and GC\_NAK2 (orange line) represents model  
5 NO<sub>2</sub> sampled from days with valid OMI data but without applying the AK. Figure 6  
6 shows almost no differences between GC\_NAK1 and GC\_NAK2 for all provinces.  
7 Therefore, the missing data have little influence on our trend analyses.

### 8 **4.3 Comparison between satellite observations and bottom-up anthropogenic** 9 **emission estimates**

10 Figure 7 shows Chinese official bottom-up provincial anthropogenic emission  
11 inventory for 2007 and 2010-2013, together with the provincial emission targets for  
12 2015 (as a goal of the 12<sup>th</sup> Five-Year Plan) (The State Council of the People's Republic  
13 of China, 2011a). Provincial mean OMI NO<sub>2</sub> VCDs are also shown for comparison.  
14 Both emission and VCD datasets were normalized to their 2007 mean values to remove  
15 the effect of regional dependence in the relation between NO<sub>x</sub> emissions and NO<sub>2</sub> VCDs.  
16 Ningxia, Xinjiang and Inner Mongolia had the largest increases in NO<sub>x</sub> emissions from  
17 2007 to 2010, consistent with their growth of NO<sub>2</sub> VCDs. NO<sub>x</sub> emissions in most  
18 provinces grew significantly from 2007 to 2010 and peaked in 2011-2012, also in  
19 general consistency with the trends in OMI NO<sub>2</sub>. On the other hand, the emission  
20 inventory suggests a reduction since 2011 for Xinjiang and Yunnan, inconsistent with  
21 the notable growth in NO<sub>2</sub> VCDs. This likely suggests an underestimate in the official  
22 emission inventory.

## 23 **5 Relating pollution changes to socioeconomic development and environmental** 24 **policies**

### 25 **5.1 General discussion on NO<sub>2</sub> trends over Western China**

26 As described in Sect. 4, the tropospheric NO<sub>2</sub> VCDs over Western China have grown  
27 notably since 2005. The growth occurred not only over cities but also over many  
28 suburban and rural regions, indicating an expansion of human influences from urban to

1 remote areas. This scale of pollution growth was associated with the rapid urbanization  
2 and industrialization over Western China following the “Go West” movement. Table 4  
3 shows that the urban population (i.e., the percentage of total population living in urban  
4 areas) increased by 10% or more from 2005 to 2013 in all provinces of Western China  
5 except Xinjiang. Over the same period, Western China experienced steep economic  
6 growth with industrial GDP growth rates of 12.4 – 20.3 % yr<sup>-1</sup> across the provinces.

7 On the other hand, the NO<sub>2</sub> VCDs declined or stabilized since 2011 in many provinces  
8 (see Fig. 6), partly reflecting some improvements in environmental strategies. China’s  
9 air pollution control strategy has been transformed from a traditional end-of-pipe  
10 control strategy (i.e., only using low NO<sub>x</sub> combustion technologies in some power  
11 plants) into a combined energy saving and emission reduction strategy after 2006 (Gu  
12 et al., 2013; Zhao et al., 2013). In particular, total NO<sub>x</sub> emissions have become a major  
13 target of national pollution control in the 12<sup>th</sup> Five-Year Plan (2011-2015), with a legally  
14 binding goal to reduce the national emissions by nearly 10% in 2015 compared to 2010  
15 (The State Council of the People’s Republic of China, 2011b). Furthermore, Chinese  
16 central government has also decided to consider the effectiveness of this reduction in  
17 evaluating local governments’ performance (The State Council of the People's Republic  
18 of China, 2012). In aspect of energy saving measures, great efforts have also been made  
19 to improve energy efficiency, to slow down growth of energy demand, and to adjust  
20 structure in various sectors (power plants, transportation, industries, and residential use)  
21 over the past few years (Wang and Hao, 2012; Zhao et al., 2013).

## 22 **5.2 On the contrast between Northwestern and Southwestern China**

23 Northwestern China (Inner Mongolia, Xinjiang, Qinghai, Gansu and Shaanxi) has an  
24 average NO<sub>2</sub> growth rate at 11.3 ± 1.0 % yr<sup>-1</sup> from 2005 to 2013, about twice the average  
25 growth rate (5.9 ± 0.6 % yr<sup>-1</sup>) in Southwestern China (Sichuan, Chongqing, Guizhou,  
26 Guangxi and Yunnan). The contrast in NO<sub>2</sub> growth rate between Northwest and  
27 Southwest reflects their distinctive states of socioeconomic development. According to  
28 the nationwide pollution census, Northwestern China generates much more NO<sub>x</sub>  
29 emissions per unit of GDP (11.94 tonnes/billion RMB in 2007) than the Southwest (6.98



1 tonnes/billion RMB) (The first nationwide pollution census committee, 2011). The  
2 difference in pollution intensities also reflects their dissimilar economic structures. In  
3 particular, Northwestern China has recently become an important energy producer (due  
4 to the “West to East Power Transmission” project) and a heavy industry base (in terms  
5 of mining, fossil fuels and raw materials)(Chen et al., 2010;Deng and Bai, 2014), and  
6 these industries are often associated with significant NO<sub>x</sub> emissions. The electricity  
7 consumption of heavy industries in Northwestern China grew by 152.5% from 2005 to  
8 2011, greater than the growth at 99.6% in Southwestern China.

9 About 70% of China’s industrial and residential energy consumption is supplied by coal  
10 burning in 2009 (Li and Leung, 2012), and the value has not changed drastically in later  
11 years. Figure 8 shows that Northwestern China has consumed more coal than the  
12 Southwest since 2005, and by 2012 their difference has increased by a factor of 35  
13 (from merely 9.03 million tonnes in 2005 to as large as 318.3 million tonnes in 2012).  
14 For the Northwest, there is an extremely high correlation between NO<sub>2</sub> VCDs and coal  
15 use across the years ( $R^2 = 0.95$ ,  $P$ -value  $< 0.05$ ), compared to a correlation at 0.84 ( $P$ -  
16 value  $< 0.05$ ) for the Southwest.

17 Furthermore, the annual amount of electricity generated by coal-fired power plants in  
18 Northwestern China increased by 237%, from 226.3 billion kWh in 2005 to 763.1  
19 billion kWh in 2013; the annual growth rates are 9.8-22.8 % yr<sup>-1</sup> for individual  
20 provinces (see Table 4). The growth was much smaller in the Southwest, about 110%  
21 from 165.6 to 347.9 billion kWh, translated to growth rates of 6.0-14.9 % yr<sup>-1</sup> for  
22 individual provinces. This difference was partly due to the stronger growth in  
23 hydropower production in the Southwest (from 147.2 to 471.6 billion kWh over 2005-  
24 2013, at the rates of 8.9-21.6 % yr<sup>-1</sup> in individual provinces) than the growth in the  
25 Northwest (from 40.0 to 107.3 billion kWh, 4.7-18.4 % yr<sup>-1</sup>).

26 Transportation plays a more important role in NO<sub>x</sub> pollution over the Southwest,  
27 compared to the Northwest. Table 4 shows that transportation contributes to much  
28 larger fractions of NO<sub>x</sub> emissions in the capital cities of Southwestern China than in the  
29 Northwestern capital cities except Xi’an, Shaanxi. In addition, the number of vehicles

1 grew faster in the Southwestern capital cities during 2005–2012.

### 2 **5.3 On the contrast between Western and Eastern China**

3 The average NO<sub>2</sub> growth rate was  $8.6 \pm 0.9\% \text{ yr}^{-1}$  for Western China, much larger than  
4 the rates in the three key eastern regions BTH ( $5.3 \pm 0.8\% \text{ yr}^{-1}$ ), YRD ( $4.0 \pm 0.6\% \text{ yr}^{-1}$ )  
5 and PRD ( $-3.3 \pm 0.3\% \text{ yr}^{-1}$ ) (see Table 1). This regional contrast reflects both their  
6 economic activities and the emission control policies adopted by the Chinese central  
7 and local governments. In particular, China's development strategy for its western  
8 provinces might have led to unintended westward pollution migration, as many  
9 resource- and pollution-intensive industries gradually moved from the East to the West  
10 after 2000. Table 4 shows that from 2005 to 2013, the average industrial GDP growth  
11 rate in Western China was  $17.2\% \text{ yr}^{-1}$  (relative to 2005), higher than the rates in the  
12 three key eastern regions ( $13.2\% \text{ yr}^{-1}$  in BTH,  $11.6\% \text{ yr}^{-1}$  in YRD and  $12.0\% \text{ yr}^{-1}$  in  
13 PRD). The fast economic and pollution growth in Western China in part reflects its  
14 growing production to support consumption in other regions (Lin et al., 2014a; Zhao et  
15 al., 2015). According to Zhao et al. (2015), NO<sub>x</sub> emissions over Western China in 2007  
16 were largely attributable to the economic production to supply Eastern China and  
17 foreign countries, with 366 Gg related to interprovincial trade and 49.1 Gg related to  
18 international trade. Together with atmospheric transport, trade has become a critical  
19 mechanism for transboundary pollution transfer at both the global and regional scales  
20 (Lin et al., 2014a), with significant consequences on public health (Jiang et al., 2015).

21 The west-east contrast in NO<sub>2</sub> growth also reflected their different pollution control  
22 strategies and measures. Although China has a national NO<sub>x</sub> emission reduction target  
23 at 10% (from 2010 to 2015), the targets are set differently for individual provinces.  
24 Table 1 shows that the targets were higher, at 13.9%, 17.7% and 16.9%, for the three  
25 key eastern regions (BTH, YRD, and PRD), but they are as low as 5.7% averaged over  
26 Western China (The State Council of the People's Republic of China, 2011a). In  
27 particular, an emission increase by 15% is allowed for Qinghai Province. In addition,  
28 although NO<sub>x</sub> emission reduction measures have been taken in power plants and some  
29 other industrial sectors since 2006 (via de-nitrification systems that involve selective

1 catalytic or non-catalytic reduction), by 2010 as much as 57% of these systems were  
2 installed in the three key eastern regions (Zhao et al., 2013). The capacity of small  
3 power generators being shut-down in Western China was about 10808 MW (excluding  
4 small diesel generators), only accounting for about 19% of the capacity of total shut-  
5 down small power plants in China (55630MW) during the 11<sup>th</sup> Five-Year Plan period  
6 (2006-2010) (NDRC, 2009-2011; Xu et al., 2013).

7 Furthermore, the vehicle emission control has also been implemented much more  
8 stringently in the East than in the West (Li and Leung, 2012). Although large amounts  
9 of “Yellow-Label Vehicles” (YLVs, highly-emitting vehicles that fail to meet the  
10 National I emission standard) have been banned from entering into big cities in Eastern  
11 China, over the recent years a considerable number of used YLVs have been brought to  
12 the West that has much weaker restrictions on YLVs (Qi, 2010). Greater efforts to  
13 reduce NO<sub>x</sub> pollution in Western China, with lessons learnt from the East, will help to  
14 achieve its sustainable development.

## 15 **6 Conclusion**

16 This study investigates the spatiotemporal variations of tropospheric NO<sub>2</sub> VCDs over  
17 Western China during 2005-2013, by using a wavelet decomposition analysis to  
18 distinguish long-term trends and other scales of temporal variability. We focus on the  
19 anthropogenic NO<sub>2</sub> by subtracting region-specific "background" values dominated by  
20 natural sources. We find that the anthropogenic NO<sub>2</sub> grew rapidly over Western China  
21 at a regional average rate of  $8.6 \pm 0.9\% \text{ yr}^{-1}$  from 2005 to 2013. Under the competing  
22 influences of economic growth and emission control, NO<sub>2</sub> levels in most western  
23 provinces increased from 2005 to 2011 and stabilized or slightly declined afterwards.  
24 GEOS-Chem model simulations and the official emission statistics are used to confirm  
25 that the OMI observed NO<sub>2</sub> trends were driven mainly by changes in anthropogenic  
26 emissions.

27 Between 2005 and 2013, Northwestern China experienced much larger NO<sub>2</sub> growth  
28 ( $11.3 \pm 1.0\% \text{ yr}^{-1}$ ) than Southwestern China ( $5.9 \pm 0.6\% \text{ yr}^{-1}$ ) and the three traditional

1 key regions of Eastern China (BTH, YRD and PRD, (-3.3)–(+5.3) % yr<sup>-1</sup>). The rapid  
2 NO<sub>2</sub> growth in Northwestern China was possibly attributed to the fast developing  
3 resource- and pollution-intensive industries along with the “Go West” movement as  
4 well as relatively weak emission controls. Rapid industrialization and urbanization in  
5 Western China should be accompanied with more stringent pollution control to achieve  
6 sustainable development.

## 7 **Acknowledgements**

8 This research is supported by the National Natural Science Foundation of China, grant  
9 41175127 and 41422502, and by the 973 program, grant 2014CB441303. We  
10 acknowledge the free use of DOMINO v2 NO<sub>2</sub> product from www.temis.nl.

## 11 **References**

- 12 Abry, P.: *Ondelettes et turbulence*, Diderot ed, Paris, 1997.
- 13 Bai, X., Shi, P., and Liu, Y.: Realizing China’s urban dream, *NATURE*, 509, 158–160,  
14 doi:10.1038/509158a, 2014.
- 15 Boersma, K. F., Eskes, H. J., Veefkind, J. P., Brinksma, E. J., van der A, R. J., Sneep,  
16 M., van den Oord, G. H. J., Levelt, P. F., Stammes, P., Gleason, J. F., and Bucsela, E. J.:  
17 Near-real time retrieval of tropospheric NO<sub>2</sub> from OMI, *Atmos. Chem. Phys.*, 7, 2103-  
18 2118, doi:10.5194/acp-7-2103-2007, 2007.
- 19 Boersma, K. F., Eskes, H. J., Dirksen, R. J., van der A, R. J., Veefkind, J. P., Stammes,  
20 P., Huijnen, V., Kleipool, Q. L., Sneep, M., Claas, J., Leitão, J., Richter, A., Zhou, Y.,  
21 and Brunner, D.: An improved tropospheric NO<sub>2</sub> column retrieval algorithm for the  
22 Ozone Monitoring Instrument, *Atmos. Meas. Tech.*, 4, 1905-1928, doi:10.5194/amt-4-  
23 1905-2011, 2011.
- 24 Chen, D., Wang, Y., McElroy, M. B., He, K., Yantosca, R. M., and Le Sager, P.: Regional  
25 CO pollution and export in China simulated by the high-resolution nested-grid GEOS-  
26 Chem model, *Atmos. Chem. Phys.*, 9, 3825-3839, doi:10.5194/acp-9-3825-2009, 2009.
- 27 Chen, W., Li, H., and Wu, Z.: Western China energy development and west to east  
28 energy transfer: Application of the Western China Sustainable Energy Development  
29 Model, *Energy Policy*, 38, 7106-7120, doi:10.1016/j.enpol.2010.07.029, 2010.
- 30 Chen, X., Feng, Y., and Huang, N. E.: Global sea level trend during 1993–2012, *Global  
31 and Planetary Change*, 112, 26-32, doi:10.1016/j.gloplacha.2013.11.001, 2014.
- 32 Daubechies, I.: *Ten Lectures on Wavelets*, CBMS-NSF Regional Conference Series in  
33 Applied Mathematics 61, Society for Industrial and Applied Mathematics,  
34 Philadelphia,PA, 377 pp., 1992.
- 35 Deng, X., and Bai, X.: Sustainable Urbanization in Western China, *Environment:*

- 1 Science and Policy for Sustainable Development, 56, 12-24,  
2 doi:10.1080/00139157.2014.901836, 2014.
- 3 Echer, E.: Multi-resolution analysis of global total ozone column during 1979-1992  
4 Nimbus-7 TOMS period, *Ann. Geophys.*, 22, 1487-1493, doi:10.5194/angeo-22-1487-  
5 2004, 2004.
- 6 Freitas, R. M., and Shimabukuro, Y. E.: Combining wavelets and linear spectral mixture  
7 model for MODIS satellite sensor time-series analysis, *Journal of Computational*  
8 *Interdisciplinary Sciences*, 1, 33-38, doi:10.6062/jcis.2008.01.01.0005, 2008.
- 9 Gu, D., Wang, Y., Smeltzer, C., and Liu, Z.: Reduction in NO<sub>x</sub> Emission Trends over  
10 China: Regional and Seasonal Variations, *Environmental Science & Technology*, 47,  
11 12912-12919, doi:10.1021/es401727e, 2013.
- 12 Hao, N., Valks, P., Loyola, D., Cheng, Y. F., and Zimmer, W.: Space-based  
13 measurements of air quality during the World Expo 2010 in Shanghai, *Environmental*  
14 *Research Letters*, 6, 044004, doi:10.1088/1748-9326/6/4/044004, 2011.
- 15 He, Y., Uno, I., Wang, Z., Ohara, T., Sugimoto, N., Shimizu, A., Richter, A., and  
16 Burrows, J. P.: Variations of the increasing trend of tropospheric NO<sub>2</sub> over central east  
17 China during the past decade, *Atmospheric Environment*, 41, 4865-4876,  
18 doi:10.1016/j.atmosenv.2007.02.009, 2007.
- 19 Huang, J., Zhou, C., Lee, X., Bao, Y., Zhao, X., Fung, J., Richter, A., Liu, X., and Zheng,  
20 Y.: The effects of rapid urbanization on the levels in tropospheric nitrogen dioxide and  
21 ozone over East China, *Atmospheric Environment*, 77, 558-567,  
22 doi:10.1016/j.atmosenv.2013.05.030, 2013.
- 23 Jiang, X., Zhang, Q., Zhao, H., Geng, G., Peng, L., Guan, D., Kan, H., Huo, H., Lin, J.,  
24 Brauer, M., Martin, R. V., and He, K.: Revealing the Hidden Health Costs Embodied in  
25 Chinese Exports, *Environmental Science & Technology*, 49, 4381-4388,  
26 doi:10.1021/es506121s, 2015.
- 27 Lamsal, L. N., Martin, R. V., Padmanabhan, A., van Donkelaar, A., Zhang, Q., Sioris,  
28 C. E., Chance, K., Kurosu, T. P., and Newchurch, M. J.: Application of satellite  
29 observations for timely updates to global anthropogenic NO<sub>x</sub> emission inventories,  
30 *Geophysical Research Letters*, 38, L05810, doi:10.1029/2010GL046476, 2011.
- 31 Li, C., Zhang, Q., Krotkov, N. A., Streets, D. G., He, K., Tsay, S.-C., and Gleason, J. F.:  
32 Recent large reduction in sulfur dioxide emissions from Chinese power plants observed  
33 by the Ozone Monitoring Instrument, *Geophysical Research Letters*, 37, L08807,  
34 doi:10.1029/2010GL042594, 2010.
- 35 Li, R., and Leung, G. C. K.: Coal consumption and economic growth in China, *Energy*  
36 *Policy*, 40, 438-443, doi:10.1016/j.enpol.2011.10.034, 2012.
- 37 Lin, J.-T., Pan, D., and Zhang, R.-X.: Trend and interannual variability of Chinese air  
38 pollution since 2000 in association with socioeconomic development: A brief overview,  
39 *Atmos. Oceanic Sci. Lett.*, 6, 84-89, 2013.
- 40 Lin, J., Nielsen, C. P., Zhao, Y., Lei, Y., Liu, Y., and McElroy, M. B.: Recent Changes

1 in Particulate Air Pollution over China Observed from Space and the Ground:  
2 Effectiveness of Emission Control, *Environmental Science & Technology*, 44, 7771-  
3 7776, doi:10.1021/es101094t, 2010a.

4 Lin, J., Pan, D., Davis, S. J., Zhang, Q., He, K., Wang, C., Streets, D. G., Wuebbles, D.  
5 J., and Guan, D.: China's international trade and air pollution in the United States,  
6 *Proceedings of the National Academy of Sciences*, 111, 1736-1741,  
7 doi:10.1073/pnas.1312860111, 2014a.

8 Lin, J. T., McElroy, M. B., and Boersma, K. F.: Constraint of anthropogenic NO<sub>x</sub>  
9 emissions in China from different sectors: a new methodology using multiple satellite  
10 retrievals, *Atmos. Chem. Phys.*, 10, 63-78, doi:10.5194/acp-10-63-2010, 2010b.

11 Lin, J. T., and McElroy, M. B.: Detection from space of a reduction in anthropogenic  
12 emissions of nitrogen oxides during the Chinese economic downturn, *Atmos. Chem.*  
13 *Phys.*, 11, 8171-8188, doi:10.5194/acp-11-8171-2011, 2011.

14 Lin, J. T.: Satellite constraint for emissions of nitrogen oxides from anthropogenic,  
15 lightning and soil sources over East China on a high-resolution grid, *Atmos. Chem.*  
16 *Phys.*, 12, 2881-2898, doi:10.5194/acp-12-2881-2012, 2012.

17 Lin, J. T., Martin, R. V., Boersma, K. F., Sneep, M., Stammes, P., Spurr, R., Wang, P.,  
18 Van Roozendaal, M., Clémer, K., and Irie, H.: Retrieving tropospheric nitrogen dioxide  
19 from the Ozone Monitoring Instrument: effects of aerosols, surface reflectance  
20 anisotropy, and vertical profile of nitrogen dioxide, *Atmos. Chem. Phys.*, 14, 1441-1461,  
21 doi:10.5194/acp-14-1441-2014, 2014b.

22 Lin, J. T., Liu, M. Y., Xin, J. Y., Boersma, K. F., Spurr, R., Martin, R., and Zhang, Q.:  
23 Influence of aerosols and surface reflectance on satellite NO<sub>2</sub> retrieval: seasonal and  
24 spatial characteristics and implications for NO<sub>x</sub> emission constraints, *Atmos. Chem.*  
25 *Phys. Discuss.*, 15, 12653-12714, doi:10.5194/acpd-15-12653-2015, 2015.

26 Martínez, B., and Gilabert, M. A.: Vegetation dynamics from NDVI time series analysis  
27 using the wavelet transform, *Remote Sensing of Environment*, 113, 1823-1842,  
28 doi:10.1016/j.rse.2009.04.016, 2009.

29 Martin, R. V., Jacob, D. J., Chance, K., Kurosu, T. P., Palmer, P. I., and Evans, M. J.:  
30 Global inventory of nitrogen oxide emissions constrained by space-based observations  
31 of NO<sub>2</sub> columns, *Journal of Geophysical Research: Atmospheres*, 108, 4537,  
32 doi:10.1029/2003JD003453, 2003.

33 Mijling, B., van der A, R. J., Boersma, K. F., Van Roozendaal, M., De Smedt, I., and  
34 Kelder, H. M.: Reductions of NO<sub>2</sub> detected from space during the 2008 Beijing  
35 Olympic Games, *Geophysical Research Letters*, 36, L13801,  
36 doi:10.1029/2009GL038943, 2009.

37 NDRC: List of Decommissioned Small Thermal Power Plants, Beijing, China, 2009-  
38 2011.

39 Partal, T., and Küçük, M.: Long-term trend analysis using discrete wavelet components  
40 of annual precipitations measurements in Marmara region (Turkey), *Physics and*

1 Chemistry of the Earth, Parts A/B/C, 31, 1189-1200, doi:10.1016/j.pce.2006.04.043,  
2 2006.

3 Percival, D. B., and Walden, A. T.: Wavelet Methods for Time Series Analysis,  
4 Cambridge University Press, 2006.

5 Qi, J.: Odd phenomenon develops in used car market, do the 'Yellow-label vehicles'  
6 restrictions work to mitigate air pollution, Xinhuanet,  
7 [http://news.xinhuanet.com/society/2010-11/28/c\\_12825457.htm](http://news.xinhuanet.com/society/2010-11/28/c_12825457.htm) (last access: 6  
8 October 2015), 2010.

9 Reuter, M., Buchwitz, M., Hilboll, A., Richter, A., Schneising, O., Hilker, M., Heymann,  
10 J., Bovensmann, H., and Burrows, J. P.: Decreasing emissions of NO<sub>x</sub> relative to CO<sub>2</sub>  
11 in East Asia inferred from satellite observations, *Nature Geosci*, 7, 792-795,  
12 doi:10.1038/ngeo2257, 2014.

13 Richter, A., Burrows, J. P., Nusz, H., Granier, C., and Niemeier, U.: Increase in  
14 tropospheric nitrogen dioxide over China observed from space, *Nature*, 437, 129-132,  
15 doi:10.1038/nature04092, 2005.

16 Rienecker, M., Suarez, M., Todling, R., Bacmeister, J., Takacs, L., Liu, H., Gu, W.,  
17 Sienkiewicz, M., Koster, R., and Gelaro, R.: The GEOS-5 Data Assimilation System—  
18 Documentation of Versions 5.0. 1, 5.1. 0, and 5.2. 0, NASA Tech. Memo, 104606, 2008,  
19 2008.

20 Russell, A. R., Valin, L. C., and Cohen, R. C.: Trends in OMI NO<sub>2</sub> observations over  
21 the United States: effects of emission control technology and the economic recession,  
22 *Atmos. Chem. Phys.*, 12, 12197-12209, doi:10.5194/acp-12-12197-2012, 2012.

23 Shao, S., and Qi, Z.: Energy Development and Economic Growth in Western China: An  
24 Empirical Analysis Based on the Resource Curse Hypothesis (in Chinese), *Economic*  
25 *Research Journal*, 4, 147-160, 2008.

26 Stavrakou, T., Müller, J. F., Boersma, K. F., De Smedt, I., and van der A, R. J.: Assessing  
27 the distribution and growth rates of NO<sub>x</sub> emission sources by inverting a 10-year record  
28 of NO<sub>2</sub> satellite columns, *Geophysical Research Letters*, 35, L10801,  
29 doi:10.1029/2008GL033521, 2008.

30 The first nationwide pollution census committee: Pollution Census Dataset, China  
31 Environmental Science Press, 2011.

32 The State Council of the People's Republic of China: The Twelfth Five-Year Plan for  
33 Energy Saving and Emission Reduction, [http://www.gov.cn/zwggk/2012-08/21/content\\_2207867.htm](http://www.gov.cn/zwggk/2012-08/21/content_2207867.htm) (last access: 10 June 2015), 2012.

35 The State Council of the People's Republic of China: Integrated Work Plan for Energy  
36 Saving and Emission Reduction During the Twelfth Five-Year Plan,  
37 [http://www.gov.cn/zwggk/2011-09/07/content\\_1941731.htm](http://www.gov.cn/zwggk/2011-09/07/content_1941731.htm) (last access: 10 June 2015),  
38 2011a.

39 The State Council of the People's Republic of China: The Twelfth Five-Year Plan for  
40 Environmental Protection, [http://www.gov.cn/zwggk/2011-12/20/content\\_2024895.htm](http://www.gov.cn/zwggk/2011-12/20/content_2024895.htm)

1 (last access: 10 June 2015), 2011b.

2 Valin, L. C., Russell, A. R., Hudman, R. C., and Cohen, R. C.: Effects of model  
3 resolution on the interpretation of satellite NO<sub>2</sub> observations, *Atmos. Chem. Phys.*, 11,  
4 11647-11655, doi:10.5194/acp-11-11647-2011, 2011.

5 van der A, R. J., Peters, D. H. M. U., Eskes, H., Boersma, K. F., Van Roozendael, M.,  
6 De Smedt, I., and Kelder, H. M.: Detection of the trend and seasonal variation in  
7 tropospheric NO<sub>2</sub> over China, *Journal of Geophysical Research: Atmospheres*, 111,  
8 D12317, doi:10.1029/2005JD006594, 2006.

9 van der A, R. J., Eskes, H. J., Boersma, K. F., van Noije, T. P. C., Van Roozendael, M.,  
10 De Smedt, I., Peters, D. H. M. U., and Meijer, E. W.: Trends, seasonal variability and  
11 dominant NO<sub>x</sub> source derived from a ten year record of NO<sub>2</sub> measured from space,  
12 *Journal of Geophysical Research: Atmospheres*, 113, D04302,  
13 doi:10.1029/2007JD009021, 2008.

14 Wang, S., and Hao, J.: Air quality management in China: Issues, challenges, and options,  
15 *Journal of Environmental Sciences*, 24, 2-13, doi:10.1016/S1001-0742(11)60724-9,  
16 2012.

17 Wang, S. W., Zhang, Q., Streets, D. G., He, K. B., Martin, R. V., Lamsal, L. N., Chen,  
18 D., Lei, Y., and Lu, Z.: Growth in NO<sub>x</sub> emissions from power plants in China: bottom-  
19 up estimates and satellite observations, *Atmos. Chem. Phys.*, 12, 4429-4447,  
20 doi:10.5194/acp-12-4429-2012, 2012.

21 Wang, Y., McElroy, M. B., Boersma, K. F., Eskes, H. J., and Veefkind, J. P.: Traffic  
22 restrictions associated with the Sino-African summit: Reductions of NO<sub>x</sub> detected from  
23 space, *Geophysical Research Letters*, 34, L08814, doi:10.1029/2007GL029326, 2007a.

24 Wang, Y., McElroy, M. B., Martin, R. V., Streets, D. G., Zhang, Q., and Fu, T.-M.:  
25 Seasonal variability of NO<sub>x</sub> emissions over east China constrained by satellite  
26 observations: Implications for combustion and microbial sources, *Journal of*  
27 *Geophysical Research: Atmospheres*, 112, D06301, doi:10.1029/2006JD007538,  
28 2007b.

29 Wang, Y., Hao, J., McElroy, M. B., Munger, J. W., Ma, H., Chen, D., and Nielsen, C. P.:  
30 Ozone air quality during the 2008 Beijing Olympics: effectiveness of emission  
31 restrictions, *Atmos. Chem. Phys.*, 9, 5237-5251, doi:10.5194/acp-9-5237-2009, 2009.

32 Witte, J. C., Schoeberl, M. R., Douglass, A. R., Gleason, J. F., Krotkov, N. A., Gille, J.  
33 C., Pickering, K. E., and Livesey, N.: Satellite observations of changes in air quality  
34 during the 2008 Beijing Olympics and Paralympics, *Geophysical Research Letters*, 36,  
35 L17803, doi:10.1029/2009GL039236, 2009.

36 Xu, Y., Yang, C.-J., and Xuan, X.: Engineering and optimization approaches to enhance  
37 the thermal efficiency of coal electricity generation in China, *Energy Policy*, 60, 356-  
38 363, doi:10.1016/j.enpol.2013.05.047, 2013.

39 Zhang, Q., Streets, D. G., He, K., Wang, Y., Richter, A., Burrows, J. P., Uno, I., Jang,  
40 C. J., Chen, D., Yao, Z., and Lei, Y.: NO<sub>x</sub> emission trends for China, 1995–2004: The



1 view from the ground and the view from space, *Journal of Geophysical Research:*  
2 *Atmospheres*, 112, D22306, doi:10.1029/2007JD008684, 2007a.

3 Zhang, Q., Streets, D. G., Carmichael, G. R., He, K. B., Huo, H., Kannari, A., Klimont,  
4 Z., Park, I. S., Reddy, S., Fu, J. S., Chen, D., Duan, L., Lei, Y., Wang, L. T., and Yao, Z.  
5 L.: Asian emissions in 2006 for the NASA INTEX-B mission, *Atmos. Chem. Phys.*, 9,  
6 5131-5153, doi:10.5194/acp-9-5131-2009, 2009a.

7 Zhang, Q., Streets, D. G., and He, K.: Satellite observations of recent power plant  
8 construction in Inner Mongolia, China, *Geophysical Research Letters*, 36, L15809,  
9 doi:10.1029/2009GL038984, 2009b.

10 Zhang, Q., Geng, G., Wang, S., Richter, A., and He, K.: Satellite remote sensing of  
11 changes in NO<sub>x</sub> emissions over China during 1996–2010, *Chinese Science Bulletin*, 57,  
12 2857-2864, doi:10.1007/s11434-012-5015-4, 2012.

13 Zhang, X., Zhang, P., Zhang, Y., Li, X., and Qiu, H.: The trend, seasonal cycle, and  
14 sources of tropospheric NO<sub>2</sub> over China during 1997–2006 based on satellite  
15 measurement, *Science in China Series D: Earth Sciences*, 50, 1877-1884,  
16 doi:10.1007/s11430-007-0141-6, 2007b.

17 Zhao, B., Wang, S. X., Liu, H., Xu, J. Y., Fu, K., Klimont, Z., Hao, J. M., He, K. B.,  
18 Cofala, J., and Amann, M.: NO<sub>x</sub> emissions in China: historical trends and future  
19 perspectives, *Atmos. Chem. Phys.*, 13, 9869-9897, doi:10.5194/acp-13-9869-2013,  
20 2013.

21 Zhao, C., and Wang, Y.: Assimilated inversion of NO<sub>x</sub> emissions over east Asia using  
22 OMI NO<sub>2</sub> column measurements, *Geophysical Research Letters*, 36, L06805,  
23 doi:10.1029/2008GL037123, 2009.

24 Zhao, H. Y., Zhang, Q., Guan, D. B., Davis, S. J., Liu, Z., Huo, H., Lin, J. T., Liu, W.  
25 D., and He, K. B.: Assessment of China's virtual air pollution transport embodied in  
26 trade by using a consumption-based emission inventory, *Atmos. Chem. Phys.*, 15, 5443-  
27 5456, doi:10.5194/acp-15-5443-2015, 2015.

28

Table 1. Regional trends of OMI NO<sub>2</sub> VCDs over 2005-2013 and NO<sub>x</sub> emission reduction plan of 2015.

	Region	Average NO <sub>2</sub> in 2005 <sup>a</sup> 10 <sup>15</sup> molecules cm <sup>-2</sup>	NO <sub>2</sub> trend <sup>b</sup> (% yr <sup>-1</sup> )	NO <sub>x</sub> emission reduction plan of 2015 (%) <sup>c</sup>
Northwest	Gansu	0.9 (0.4, I)	7.5 ± 1.2	3.1
	Inner Mongolia	1.1 (0.4, I)	10.2 ± 1.3	5.8
	Ningxia	1.4 (0.4, I)	12.3 ± 1.7	4.9
	Qinghai	1.0 (0.5, II)	11.2 ± 1.2	-15.3
	Shaanxi	2.3 (0.5, II)	10.5 ± 1.0	9.9
	Xinjiang	1.0 (0.5, II)	15.1 ± 2.0	0
Southwest	Chongqing	2.2 (0.5, III)	7.8 ± 0.9	6.9
	Guangxi	1.2 (0.5, III)	4.0 ± 0.5	8.8
	Guizhou	1.3 (0.5, III)	6.9 ± 1.0	9.8
	Sichuan	1.7 (0.5, III)	6.1 ± 0.7	6.9
	Yunnan	0.7 (0.5, III)	4.2 ± 0.3	5.8
Region	West	1.3 (0.5, II)	8.6 ± 0.9	5.7
	Northwest	1.2 (0.5, II)	11.3 ± 1.0	4.5
	Southwest	1.4 (0.5, III)	5.9 ± 0.6	7.6
	BTH	9.2 (0.7, IV)	5.3 ± 0.8	13.9
	YRD	7.2 (1.2, V)	4.1 ± 0.6	17.7
	PRD	8.0 (1.2, VI)	-3.3 ± 0.3	16.9

- All the provincial NO<sub>2</sub> data have been subtracted by its respective “background” values. The “background” values and regions are indicated in the parentheses.
- NO<sub>2</sub> trends are derived from the *A5* time series. All trend values are relative to 2005 and are statistically significant.
- NO<sub>x</sub> reduction represents the proposed emissions in 2015 relative to 2010. The value for PRD refers to the proposed target for Guangdong Province. Qinghai Province is allowed to emit more NO<sub>x</sub> in 2015 compared to 2010.

Table 2. Linear regression for GEOS-Chem modeled annual mean NO<sub>2</sub> VCDs as a function of OMI values over China and Western China.

Year	2005	2006	2007	2008	2009	2010	2011	2012
China								
Slope	1.11	1.18	1.19	1.09	1.15	1.17	1.26	1.22
Intercept	0.26	0.33	0.36	0.32	0.27	0.32	0.31	0.21
R <sup>2</sup>	0.88	0.86	0.89	0.88	0.88	0.89	0.90	0.89
Western China								
Slope	1.17	1.16	1.22	1.08	1.19	1.18	1.23	1.26
Intercept	-0.05	0.07	0.01	0.03	-0.08	-0.01	0.00	-0.13
R <sup>2</sup>	0.70	0.68	0.71	0.72	0.74	0.76	0.76	0.75

Table 3. Percentage changes in modeled NO<sub>2</sub> from 2005 to 2012.

Region		With changes in anthropogenic emissions	Without changes in anthropogenic emissions
Northwest	Gansu	70.9	-8.4
	Inner-Mongolia	129.3	21.9
	Ningxia	94.9	-1.2
	Qinghai	102.2	12.6
	Shaanxi	81.6	-6.6
	Xinjiang	51.8	1.5
Southwest	Chongqing	54.1	-2.7
	Guangxi	27.0	-16.6
	Guizhou	71.1	3.2
	Sichuan	52.2	-5.1
	Yunnan	9.4	-10.7
Region	West	70.4	1.6
	Northwest	85.8	6.9
	Southwest	46.8	-6.3
	BTH	62.5	1.9
	YRD	40.4	3.2
	PRD	-30.4	-0.6

Table 4. Socioeconomic statistics for individual provinces and capital cities.

Region	Provincial-level regions	Urban population in 2005 (% of total)	Urban population in 2013 (% of total)	Industrial GDP annual growth rate for 2005-2013 (% yr-1)	Thermal power generation annual growth rate for 2005-2013 (% yr-1)	Hydropower generation annual growth rate for 2005-2013 (% yr-1)	Capital cities <sup>a</sup>	Increase in vehicle ownership between 2005 and 2012 (million vehicles)	Percentage of transportation to total NO <sub>x</sub> emissions (%)
Northwest	Gansu	30.0	40.1	13.8	9.8	9.9	Lanzhou	-	21.1
	Inner Mongolia	47.2	58.7	20.3	16.9	15.0	Hohhot	0.41	17.5
	Ningxia	42.3	52.0	15.0	17.9	7.2	Yinchuan	0.18	21.3
	Qinghai	39.3	48.5	16.0	12.0	13.2	Xining	0.03	27
	Shaanxi	37.2	51.3	17.0	14.0	4.7	Xi'an	1.09	56.6
	Xinjiang	37.2	44.5	12.4	22.8	18.4	Urumqi	0.37	25.7
Southwest	Chongqing	45.2	58.3	19.4	11.2	14.5	Chongqing	2.79	40.9
	Guangxi	33.6	44.8	17.4	14.9	11.2	Nanning	0.6	47.7
	Guizhou	26.9	37.8	14.0	9.9	8.9	Guiyang	0.44	26.4
	Sichuan	33.0	44.9	18.5	6.0	15.4	Chengdu	1.56	46.9
	Yunnan	29.5	40.5	14.6	7.0	21.6	Kunming	1.02	34.1

a. Vehicle data for Lanzhou are unavailable.

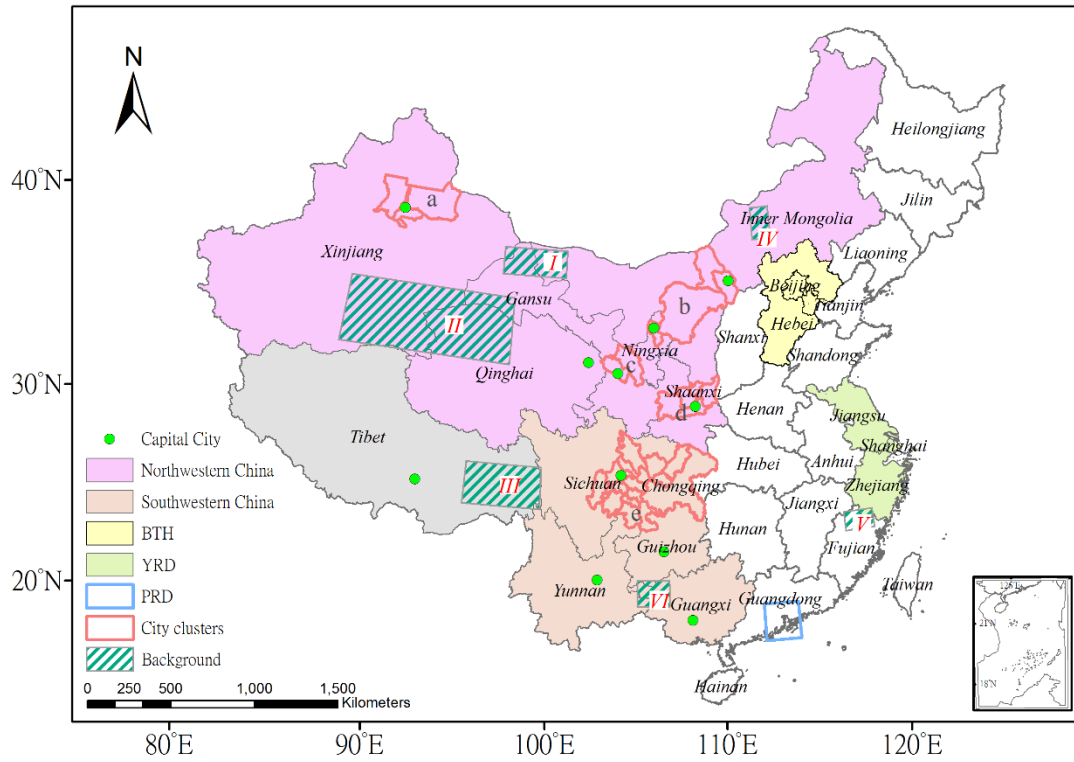


Figure 1. The study regions. Several city clusters are also identified: (a) Urumqi city cluster, (b) Inner Mongolia industrial city cluster, (c) Gansu-Ningxia, (d) Shaanxi-Guanzhong, and (e) Chengdu-Chongqing.

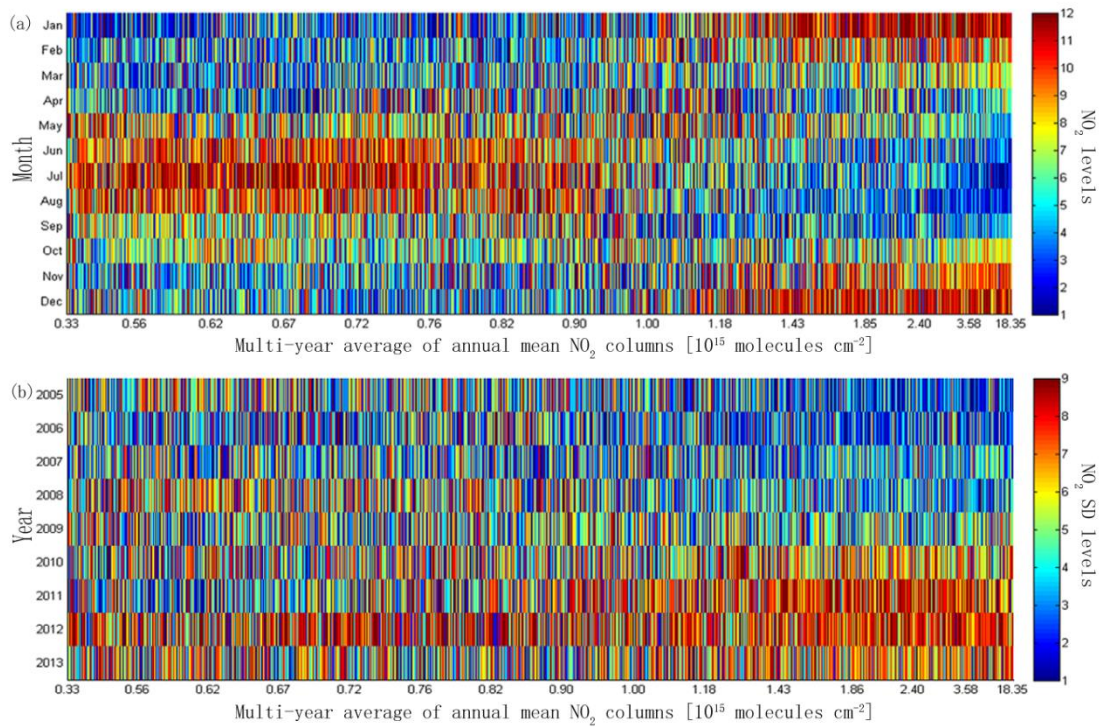


Figure 2. (a) 2005-2013 average seasonal variation of OMI NO<sub>2</sub> VCDs for each 0.25° x 0.25° grid cell of Western China; the grid cells are sorted by their 9-year average NO<sub>2</sub> VCDs. For each grid cell, the 9-year average monthly NO<sub>2</sub> values are converted to their reverse ranks (from 1 to 12; 1 represents the smallest NO<sub>2</sub> value). (b) Standard deviation (SD) of monthly OMI NO<sub>2</sub> VCDs in individual years over 2005 – 2013 for each 0.25° x 0.25° grid cell of Western China; the grid cells are sorted by their 9-year average NO<sub>2</sub> VCDs. For each grid cell, the seasonal SDs in the nine years are converted to their reverse ranks (from 1 to 9; 1 represents the smallest SD value).

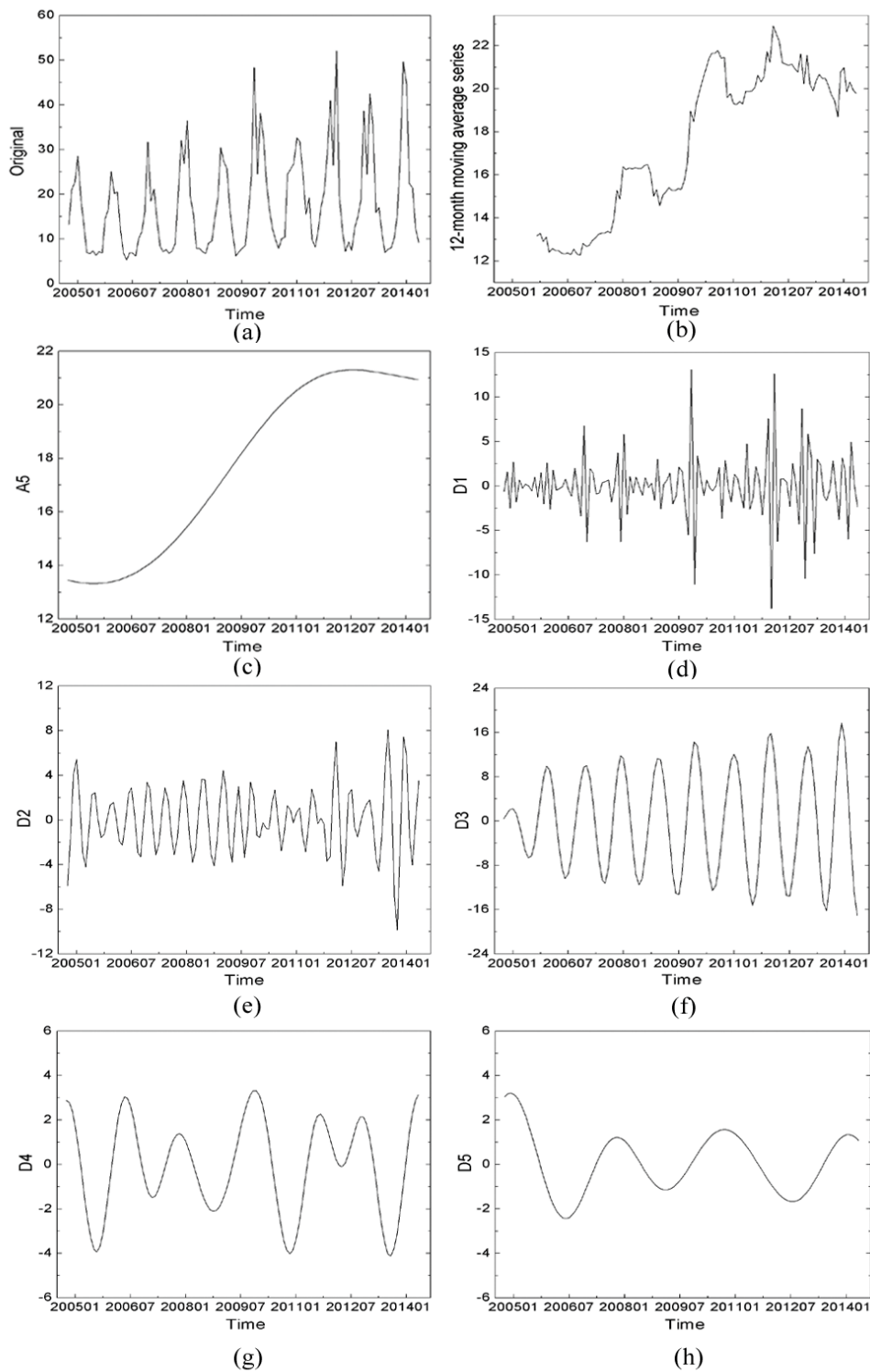


Figure 3. An example of the 5-level wavelet decomposition. (a) The original monthly time series of OMI NO<sub>2</sub> at a grid cell in Xi'an (34.5°N, 108.9°E), (b) The 12-month moving average time series, (c) The approximation signal  $A_5$  representing the long-term trend, (d)-(h) Five decomposition levels  $D_1$ - $D_5$  indicating temporal variability at various scales.



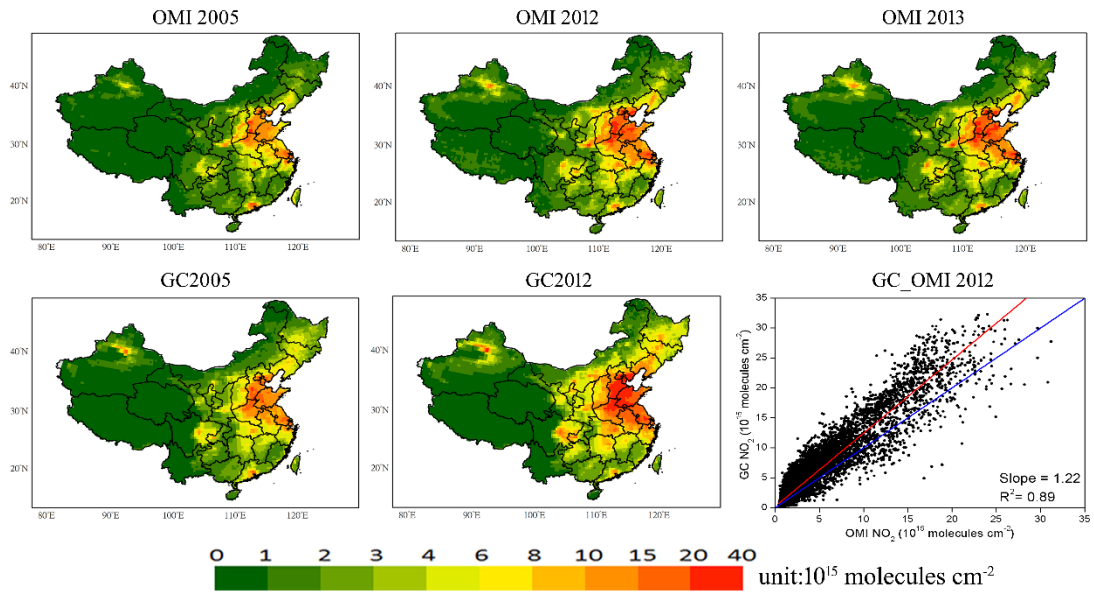


Figure 4. Annual mean OMI NO<sub>2</sub> VCDs over China in 2005, 2012 and 2013, annual mean GEOS-Chem NO<sub>2</sub> VCDs in 2005 and 2012, and a scatterplot with linear regression for model vs. OMI NO<sub>2</sub> in 2012. In the scatterplot, the red line represents a linear fit, and the blue line is the 1:1 line.

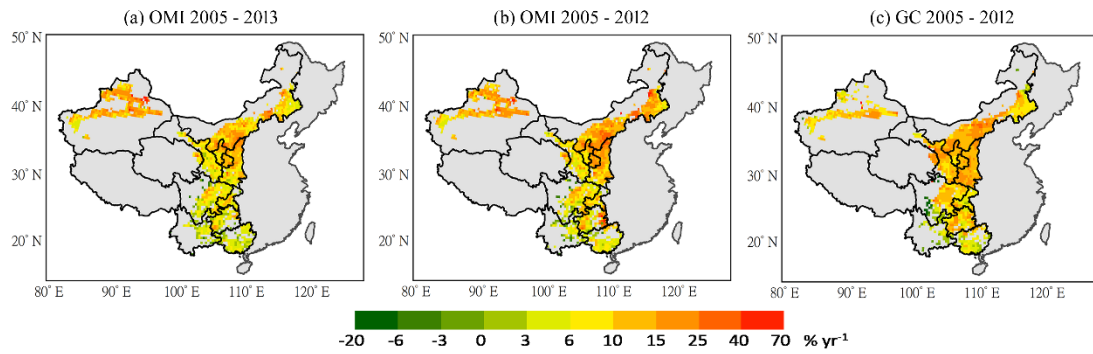


Figure 5. Percentage trends of annual mean OMI and Model NO<sub>2</sub> VCDs over Western China (relative to 2005), by applying a linear regression to the approximation signal  $A_5$  from the wavelet decomposition. All the NO<sub>2</sub> data have been subtracted by their respective “background” values prior to the wavelet decomposition. Results are shown only for grid cells with 2005-2013 average NO<sub>2</sub> VCDs exceeding  $1.0 \times 10^{15}$  molecules  $\text{cm}^{-2}$  and with statistically significant trends ( $P$ -value  $< 0.05$  according to an  $F$ -test). (a) OMI NO<sub>2</sub> trends from 2005 to 2013, (b) OMI NO<sub>2</sub> trends from 2005 to 2012, (c) Model NO<sub>2</sub> trends from 2005 to 2012.

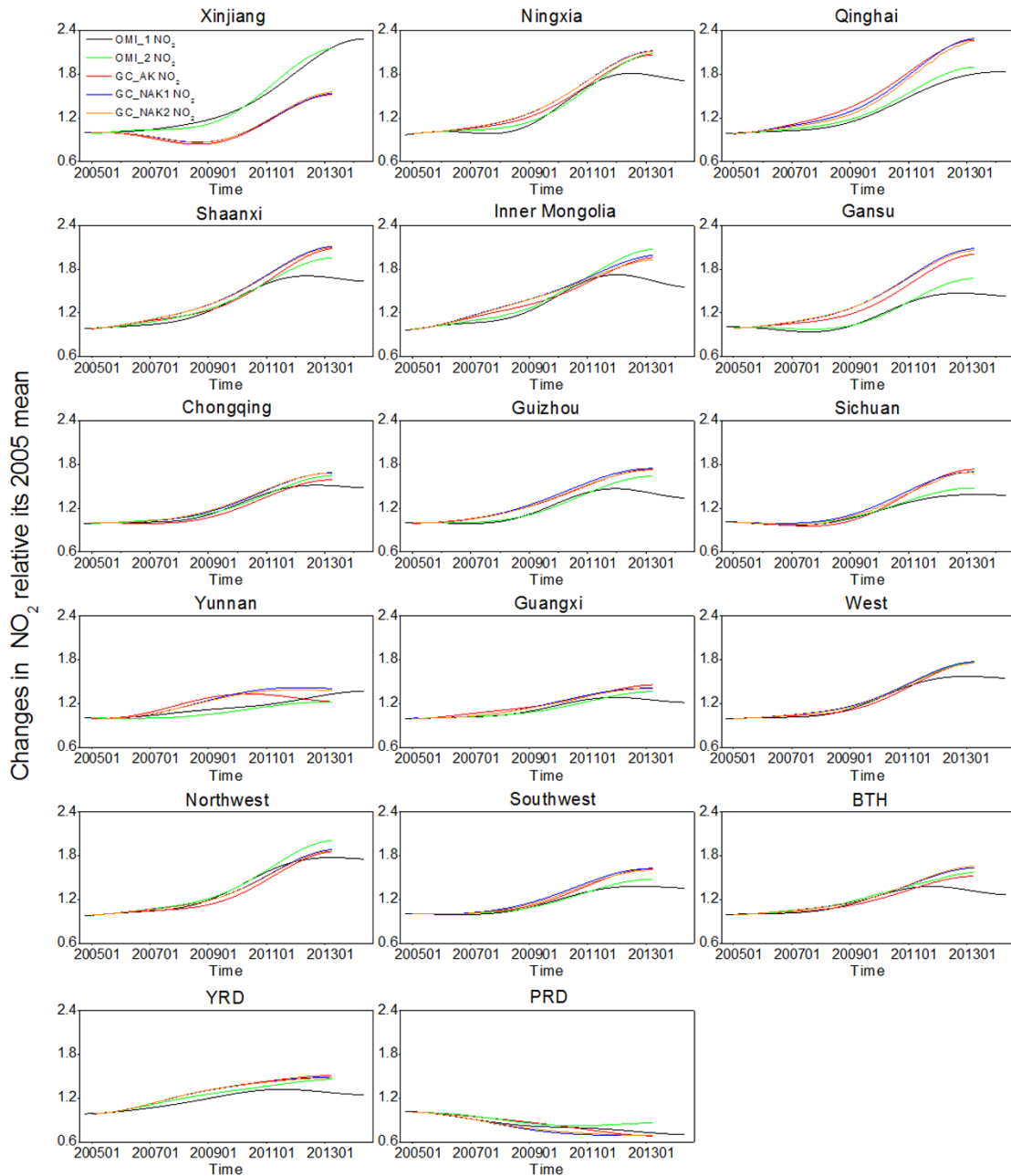


Figure 6. The long-term trends (i.e., the  $A5$  component out of the wavelet analysis) of OMI and modeled  $\text{NO}_2$  in individual provinces and regions. The values are normalized to 2005. OMI\_1 (black line) denotes the  $A5$  signal from a wavelet analysis of OMI  $\text{NO}_2$  over Oct 2004 – May 2014, and OMI\_2 (green line) corresponds to the wavelet analysis over Jan 2005 – Apr 2013. GC\_AK (red line) corresponds to a wavelet analysis of coincident modeled values (applied with the AK) over Jan 2005 – Apr 2013. GC\_NAK1 (blue line) represents the  $A5$  signal for modeled  $\text{NO}_2$  on all days (without applying the AK) over Jan 2005 – Apr 2013, and GC\_NAK2 (orange line) is similar to GC\_NAK1 but with model results coincident with valid OMI data.

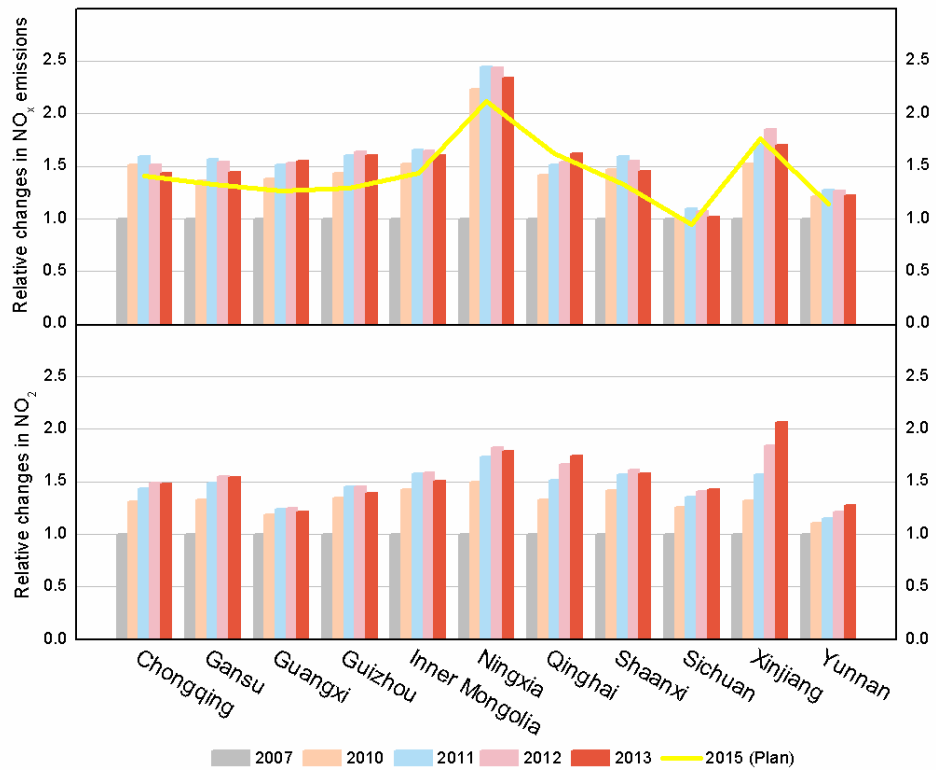


Figure 7. Relative Changes in OMI NO<sub>2</sub> VCDs and NO<sub>x</sub> emissions in 2007 and 2010-2013 (relative to 2007). (Top) Chinese official provincial-level NO<sub>x</sub> emission inventory for 2007 and 2010-2013 as well as its targeted emissions for 2015. (Bottom) Annual mean OMI NO<sub>2</sub> levels in 2007 and 2010-2013.

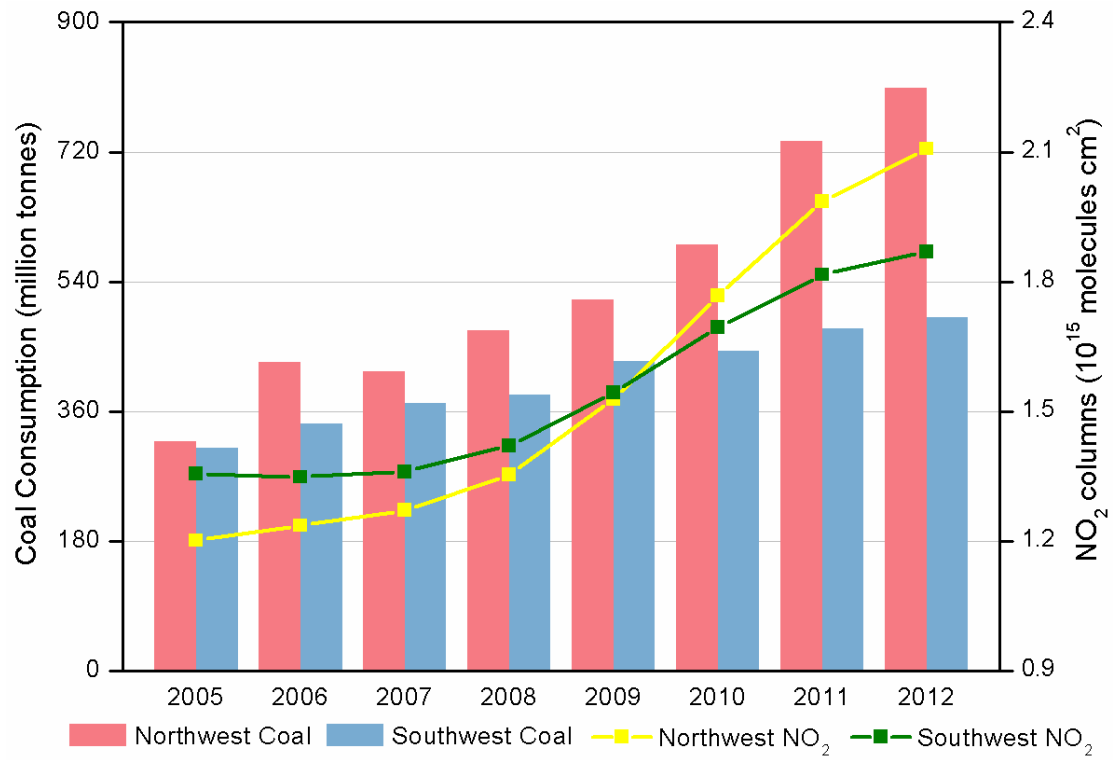


Figure 8. Coal consumption and annual mean OMI NO<sub>2</sub> levels over Western China.